Contrib Mineral Petrol (2012) 163:841–860
DOI 10.1007/s00410-011-0702-8

ORIGINAL PAPER

Heterogeneous mantle source and magma differentiation of quaternary arc-like volcanic rocks from Tengchong, SE margin of the Tibetan Plateau

Mei-Fu Zhou · Paul T. Robinson · Christina Yan Wang · Jun-Hong Zhao · Dan-Ping Yan · Jian-Feng Gao · John Malpas

Received: 8 June 2011 / Accepted: 18 October 2011 / Published online: 3 November 2011

Abstract The Tengchong volcanic field north of the Burma arc comprises numerous Quaternary volcanoes in the southeastern margin of the Tibetan Plateau. The volcanic rocks are grouped into four units (1–4) from the oldest to youngest. Units 1, 3 and 4 are composed of olivine trachybasalt, basaltic trachyandesite and trachyandesite, and Unit 2 consists of hornblende dacite. The rocks of Units 1, 3, and 4 form a generally alkaline suite in which the rocks plot along generally linear trends on Harker diagrams with only slight offset from unit to unit. They contain olivine phenocrysts with Fo values ranging from 65 to 85 mol% and have Cr-spinel with Cr# ranging from 23 to 35. All the rocks have chondrite-normalized REE patterns enriched in LREE and primitive mantle-normalized trace element patterns depleted in Ti, Nb and Ta, but they are rich in Th, Ti and P relative to typical arc volcanics. Despite minor crustal contamination, $^{87}Sr/^{86}Sr$ ratios (0.706–0.709), εNd values (−3.2 to −8.7), and εHf values (+4.8 to −6.4) indicate a highly heterogeneous mantle source. The Pb isotopic ratios of the lavas ($^{206}Pb/^{204}Pb = 18.02–18.30$) clearly show an EMI-type mantle source. The underlying mantle source was previously modified by subduction of the Neo-Tethyan oceanic and Indian continental lithosphere. The present heterogeneous mantle source is interpreted to have formed by variable additions of fluids and sediments derived from the subducted Indian Oceanic lithosphere, probably the Ninety East Ridge. Magma generation and emplacement was facilitated by transtensional NS-trending strike-slip faulting.

Keywords Arc-like volcanic rocks · Heterogeneous mantle source · Sr–Nd–Pb–Hf isotopes · Magma chamber processes · Tengchong · SE margin of the Tibetan Plateau

Communicated by T. L. Grove.

Electronic supplementary material The online version of this article (doi:10.1007/s00410-011-0702-8) contains supplementary material, which is available to authorized users.

M.-F. Zhou (✉)
Key Laboratory of Ore Deposit Geochemistry,
Institute of Geochemistry, Chinese Academy of Sciences,
Guiyang, China
e-mail: mfzhou@hkucc.hku.hk

M.-F. Zhou · P. T. Robinson · J.-F. Gao · J. Malpas
Department of Earth Sciences, The University of Hong Kong,
Hong Kong, China

C. Y. Wang
Key Laboratory of Mineralogy and Metallogeny, Guangzhou
Institute of Geochemistry, Chinese Academy of Sciences,
Guangzhou 510640, China

J.-H. Zhao
State Key Laboratory of Geological Processes and Mineral
Resources, China University of Geosciences, Wuhan 430074,
People's Republic of China

D.-P. Yan
State Key Laboratory of Geological Processes and Mineral
Resources, China University of Geosciences, Beijing 430074,
People's Republic of China

Introduction

Syn- and post-collisional igneous activities in the Tibetan Plateau record the evolution of the underlying mantle and lower crust. Previous studies have documented extensive magmatism related to the subduction of Neo-Tethyan oceanic lithosphere and the Indian continental crust (e.g., Turner et al. 1996; Ding et al. 2003; Chung et al. 2005; Mo

et al. 2006; 2007). In SW China and Burma, along the southeastern margin of the plateau, recent volcanism is associated with strike-slip fault systems. Two volcanic fields are recognized: one to the north of Wuntho, Central Burma (Stephenson 1984) and one in Tengchong, western Yunnan, SW China (Fig. 1). The lavas include high-K, calc-alkaline to weakly shoshonitic, volcanic rocks, superficially similar to those of arc volcanoes. However, they have very complex geochemical and isotopic compositions, suggesting derivation from a highly variable and composite source.

A major Mesozoic suture zone, considered to be the extension of the Yarlung-Zangbo suture in Tibet, lies between these two volcanic fields (Fig. 1), and the Kohima suture to the west probably marks an east-dipping, continental subduction zone. Concurrent, ongoing northward subduction of the Indian Ocean lithosphere has created the active Burma-Sunda volcanic arc to the south (Fig. 1). The convergence of these systems in southwest China and Burma has produced a region with a very complex tectonic history. Little detailed information is available for either the Tengchong or Wuntho lavas, and nothing is known about the nature of the underlying mantle.

Pliocene to Recent volcanic activity in the Tengchong area is recorded in numerous small cinder cones and associated lava flows (Fig. 2). The most recent eruption was in 1609 (Xu 1939), and the volcanoes are considered to be active based on on-going geothermal and earthquake activity. The lavas at Tengchong comprise three units of mafic and intermediate rocks (trachybasalt, basaltic trachyandesite, and trachyandesite) and one unit of dacite. The earliest description of the volcanoes is in a report by Xiake Xu, a noted Chinese geographer, published in 1639 (Xu 1939; also see Liu 1999). The volcanoes were also described by Anderson (1871, 1876), Széchenyi (1893), Brown (1913), Zhang (1924) and Chang (1948). Modern scientific investigation of these rocks by Zhu et al. (1983) suggested that the most voluminous lavas were produced

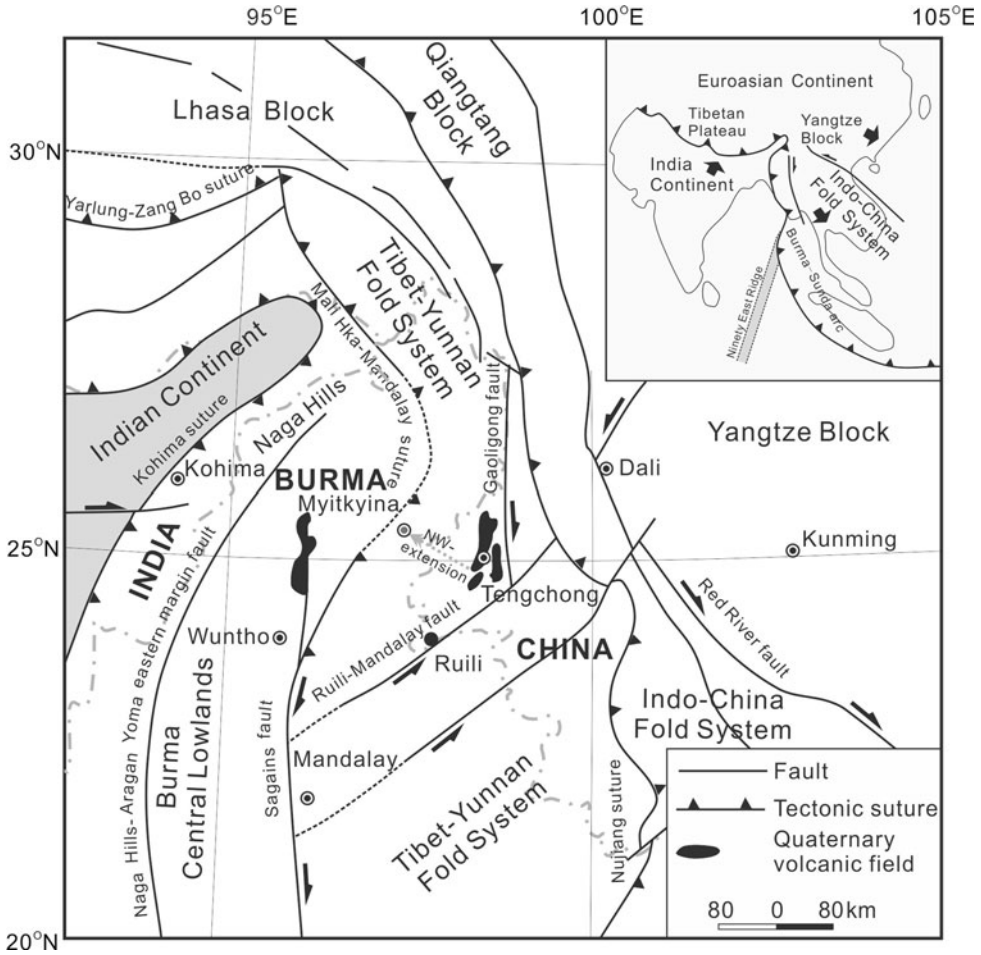

Fig. 1 A simplified geological map showing major tectonic units in the collisional zone between the Indian and Eurasian plates (after Tapponnier et al. 1982; McCaffrey 2009) and the location of the Tengchong volcanic field in SW China. Also shown is the location of the Quaternary volcanic field north of Wuntho, Burma

by partial melting of a metasomatized mantle source. Mu et al. (1987a) argued that the isotopic and geochemical characteristics of the rocks point to a continental component derived either by assimilation or by recycling of crustal material into the magma source. Cong et al. (1994) and Wang et al. (2006) suggested that the rocks were derived by partial melting of a metasomatized mantle source previously modified by oceanic subduction at ~65 Ma. Wang et al. (2006) recognized two source domains for the lavas; one that produced a LREE-enriched, high Rb/Sr end-member marked by ^{230}Th enrichment and the other that produced a typical arc-type melt with lower ^{230}Th. These studies demonstrated that the volcanic rocks in the southeast most margin of the Tibetan Plateau have arc-like characteristics but that they are more K-rich than typical arc assemblages and are significantly different from volcanic rocks elsewhere in the plateau.

The eruption of the Tengchong volcanoes north of the Burma arc raises many questions regarding the nature of the mantle source, composition of parental magma(s), the roles of crustal contamination and fractional crystallization in the magma evolution, the source of the heat that triggered melting and the nature of the overall tectonic environment in which the volcanoes formed. Answers to these questions are obscure because no integrated study of the petrology, mineralogy and geochemistry of these rocks is available.

In this paper, we describe the most primitive lavas that erupted during three stages of volcanic activity. The dacite unit involved crustal melting and is not considered in this paper. The new data set including mineral chemistry and whole-rock major oxide, trace element and Sr–Nd–Pb–Hf isotopic compositions is used to document some unique features of the volcanic rocks compared with typical arc rocks and to identify a highly heterogeneous mantle source that was modified by variable amounts of subduction components. We propose that the underlying mantle was originally modified by subduction of Neo-Tethyan Oceanic lithosphere followed by subduction of the Indian continental lithosphere (~40 Ma). The modern activity in Tengchong records recent modification of the mantle by subduction of present-day Indian Ocean lithosphere, perhaps including the Ninety East Ridge.

Geological background

The Tibetan Plateau consists of the Kunlun, Songpan-Ganzi, Qiangtang, and Lhasa terranes to the north and the Indian sub-continent to the south. These terranes were successively accreted to the Asian continent since the Paleozoic. Sinistral strike-slip motion along several major faults accommodated southeastward escape of the Tibetan Plateau since ~27 Ma (Tapponnier et al. 1982; Socquet and Pubellier 2005) and continues to the present time. The major terranes extend to the east and southeast, partially due to this extrusion of the plateau.

In the southeastern margin of the plateau, from west to east, these terranes include the Indian continent, Tibet-Yunnan Fold System, Indo-China Fold System and Yangtze Block, all of which are separated by major faults (Fig. 1; Yan et al. 2006). The Tibet-Yunnan Fold System is separated from the Yangtze Block by the Red-River fault to the east and from the Burma Central Lowlands to the west by the Mali Hka-Mandalay suture (Fig. 1). This suture extends to the Indus-Yarlung Zangbo suture zone in the northwest and is marked by ophiolites formed in the Neo-Tethyan Ocean. Farther to the west, the Burma Central Lowlands are separated from the Indian continent by the Kohima suture, which extends to the main boundary thrust to the northwest (Fig. 1).

The collision between the Asian and Indian continents was associated with extensive magmatism. The subduction of Neo-Tethyan Oceanic lithosphere produced the Gangdese granitoid batholiths and the 5-km-thick Linzizong volcanic succession (Chung et al. 2005; Mo et al. 2007). In the Tengchong area, the 68–53 Ma granites emplaced at are considered to be the continuation of the Gangdese magmatic arc of the Lhasa terrane.

Post-collisional volcanism began immediately after the collision and has continued to the present (Turner et al. 1996; Ding et al. 2003; Nomade et al. 2004; Williams et al. 2004; Chung et al. 2005; Guo et al. 2006; Mo et al. 2006; Zhao et al. 2009). This magmatism generated potassic to ultrapotassic volcanic rocks in the Lhasa and Qingtang terranes. High-potassium igneous rocks are also widespread along the Red River fault, just north of the Tengchong region (Wang et al. 2001). They show Sr–Nd isotopic compositions that resemble those of the Indian crustal basement. This has been taken as evidence for subduction of the Indian continental crust underneath the Lhasa terrane since the Oligocene (Zhao et al. 2003; 2009; Guo et al. 2006).

The Tengchong volcanic field in the Tibet-Yunnan Fold System is located within pull-apart basins produced in a stress field of NNE-NE-compression and WNW-NW-extension (Wang et al. 2007). The volcanoes occur along the Gaoligong dextral strike-slip fault near its intersection with the Ruili-Mandalay sinistral strike-slip fault (Fig. 1). The Gaoligong metamorphic complex is exposed in the Gaoligong mountain range to the east (YBGMR 1979) and is thought to form the basement in the region. The basement complex is intruded by numerous Late Mesozoic to early Cenozoic arc granites (YBGMR 1979) and overlain by pre-Quaternary sedimentary strata.

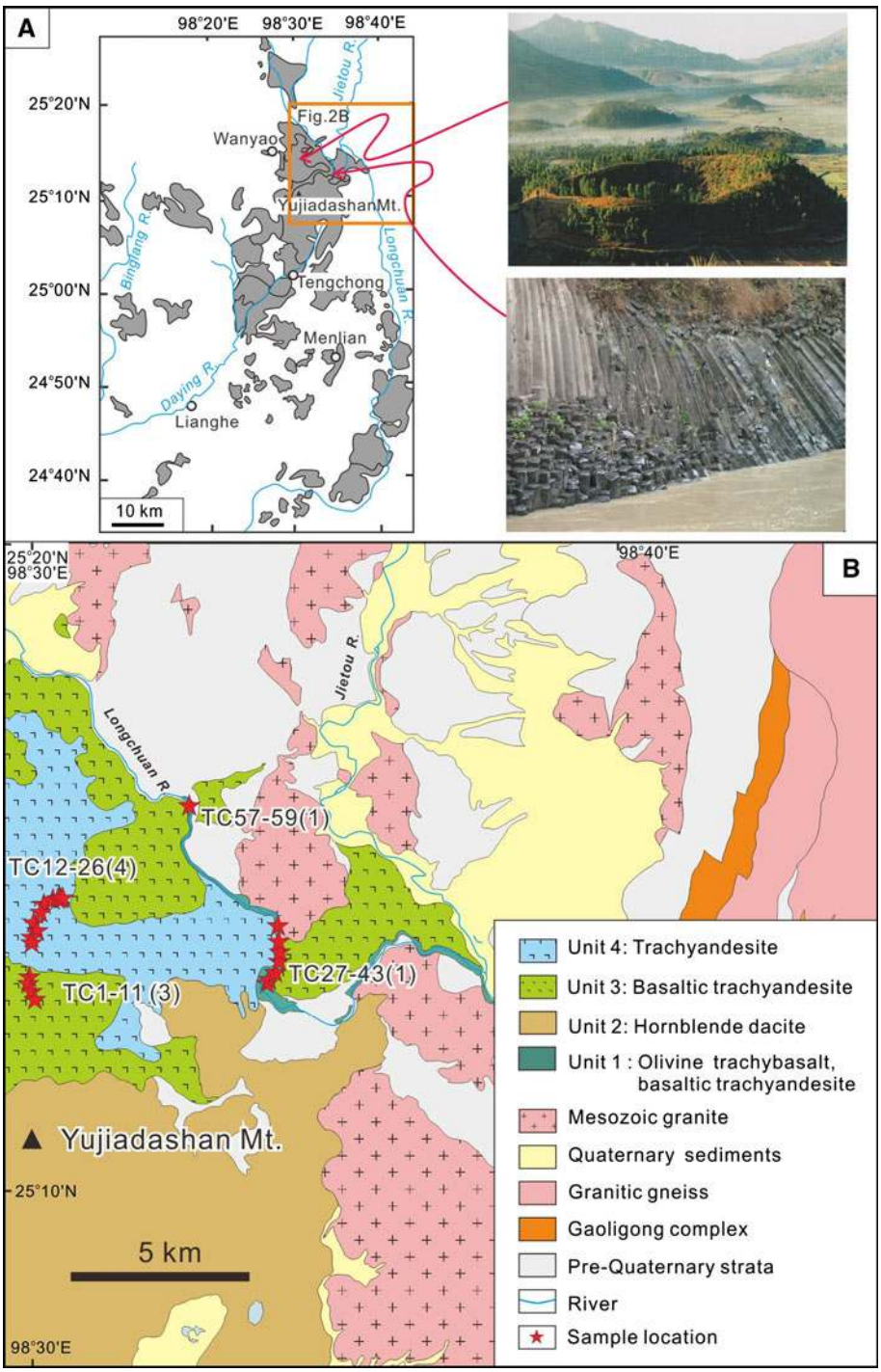

Fig. 2 Distribution of Quaternary lavas in the Tengchong volcanic field (**a**) and sampling locations (**b**). Four eruption units are recognized (1–4), from oldest to youngest (adopted from an unpublished geological map of 1:50,000 scale by Geological Survey of Yunnan 2000)

Field relations and petrography of volcanic rocks

In the Tengchong volcanic field, the volcanoes are distributed in an area ~90 km long from north to south and ~30 km wide (Fig. 2). More than 90 individual cones are recognized (Fig. 2), and many of these are associated with short, stubby flows, up to about 35 m thick, which typically show well-developed columnar jointing (Fig. 2).

Based on ^{230}Th–^{238}U, K/Ar and thermoluminescence dating, the Tengchong volcanic rocks range in age from 5.5 Ma to present (Mu et al. 1987a, b; Li et al. 2000; Yin and Li 2000; Wang et al. 2006). However, many of these dates are of unknown quality, and most of the rocks are very young. The most recent eruption was in 1609, and the field is considered to still be active.

According to rock types, four principal lithologic units are recognized in the Tengchong area (Fig. 2). Unit 1,

generally considered the oldest, consists chiefly of olivine trachybasalt and basaltic trachyandesite, whereas a distinct sequence of hornblende dacite makes up Unit 2. Relatively uniform basaltic trachyandesite comprises Unit 3, and Unit 4, the youngest, consists of trachyandesite.

Units 1 and 3 lavas are fine-grained, moderately phyric, sparsely vesicular, lavas (see Electronic Appendix 1). Phenocrysts of olivine, plagioclase and sparse augite make up ~10–15 modal% and are set in fine-grained, intersertal to intergranular groundmass. The olivine phenocrysts exhibit both oscillatory and reverse zoning with Fo values ranging from 84 to 75, whereas the groundmass olivine has Fo values ranging from 64 to 59 (Appendix 2). Some of the olivine phenocrysts contain small chromite inclusions with Cr#s (100Cr/(Cr + Al)) of 23–35 and Mg#s (100 Mg/(Mg + Fe^{2+})) of 45–67 (Appendix 3). On a plot of TiO_2 versus Al_2O_3, the chromite grains all plot in, or near, the MORB field and have much higher Al_2O_3 than chromites from island arc, OIB and LIP mafic–ultramafic rocks and much higher TiO_2 than island arc volcanic rocks and depleted mantle peridotites (Fig. 3). Plagioclase compositions are similar in both Units 1 and 3, generally ranging from An_{68} to An_{59} in the large phenocrysts and from An_{63} to An_{55} in the groundmass (Appendix 4). Some very large plagioclase phenocrysts in Unit 1 exhibit reverse zoning. Clinopyroxene is abundant in the groundmass of Units 1 and 3 and also forms small phenocrysts (Appendix 1). It has a relatively uniform composition, ranging from $En_{48}Fs_{10}Wo_{42}$ to $En_{44}Fs_{15}Wo_{41}$ (Appendix 5). Minute crystals of magnetite and ilmenite are also common in the groundmass (Appendix 3).

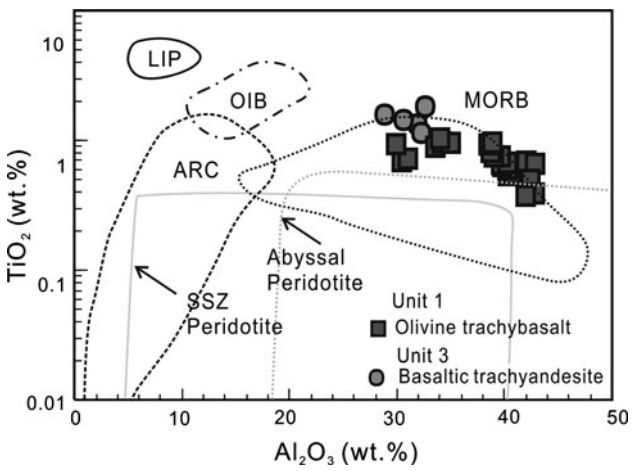

Fig. 3 Plots of Al_2O_3 versus TiO_2 of chromite from the lavas at Tengchong. Reference fields after Kamenetsky et al. (2001). *LIP* large igneous provinces, *OIB* intra-plate ocean islands, *ARC* island arcs, *MORB* mid-ocean ridge basalts, *SSZ peridotite* spinel from supra-subduction zone, and abyssal peridotite-spinel from mid-ocean ridge

The rocks of Unit 2 are fine-grained, moderately phyric, hornblende dacite (Appendix 1). They contain 20–25 modal% phenocrysts, chiefly plagioclase and hornblende, with minor amounts of biotite and pyroxene, all set in a glassy groundmass. Small plagioclase phenocrysts are accompanied by relatively large corroded plagioclase xenocrysts with reverse zoning. The hypersthene laths are commonly corroded and rimmed, or partly replaced by, clinopyroxene or hornblende. These features suggest a complex origin of the dacite involving crustal melting, and this unit will not be discussed further in this paper.

Unit 4 consists of very fine-grained, moderately to weakly porphyritic, trachyandesites with a glassy groundmass. Phenocrysts make up ~5–12 modal% and consist chiefly of pyroxene with lesser amounts of plagioclase (Appendix 1). The plagioclase phenocrysts range from An_{63} to An_{49}, with the large crystals being more calcic than the smaller ones. Plagioclase in the groundmass has a narrow range of composition ($An_{55–52}$; Appendix 4). Most of the pyroxene is augite ($En_{44–48}$), but some laths of hypersthene ($En_{74–77}$; Appendix 4) are also present and many of them have narrow rims of augite. A few of larger hypersthene grains have narrow exsolution lamellae of clinopyroxene. All of the rocks are very fresh with no observable secondary minerals. A single olivine xenocryst in Unit 4 is normally zoned from Fo_{77} in the core to Fo_{73} in the rim.

The rocks of Units 1, 3 and 4 all contain 1–5 modal% of xenocrysts, chiefly plagioclase and quartz (Appendix 1). The plagioclase xenocrysts occur as anhedral to subhedral laths up to 5 mm long, with fritted margins, some of which are surrounded by clear overgrowth rims. A few of the grains also have strongly pitted cores. Quartz forms small, subrounded grains, 0.3–0.5 mm across, which are commonly rimmed with clinopyroxene (Appendix 1). One sample (TC-6) has numerous clots of fine-grained pyroxene, 0.2–0.3 mm across, that were probably originally small quartz xenocrysts.

Analytical techniques

Major and trace elemental analyses

Whole-rock major oxides were analyzed by X-ray fluorescence on fused glass beads at The University of Hong Kong, following the analytical procedures of Zhou et al. (2006). Analytical precision is better than 1% for SiO_2 and better than 2% for the other oxides. Trace elements were analyzed by inductively coupled plasma-mass spectrometry (ICP-MS) also at The University of Hong Kong, according to procedures described by Zhou et al. (2006). Analytical precision for most elements is better than 5%.

Sr–Nd–Pb–Hf isotope analyses

Whole-rock Sr–Nd–Pb–Hf isotopes were measured at the Institute of Geology and Geophysics, Chinese Academy of Sciences. Sr–Nd isotopes were analyzed with a Finnigan MAT 262 thermal ionization mass spectrometer. Measured $^{87}Sr/^{86}Sr$ and $^{143}Nd/^{144}Nd$ ratios were normalized to $^{86}Sr/^{88}Sr = 0.1194$ and $^{146}Nd/^{144}Nd = 0.7219$, respectively. The reported $^{87}Sr/^{86}Sr$ and $^{143}Nd/^{144}Nd$ ratios were adjusted to the NBS SRM 987 standard $^{87}Sr/^{86}Sr = 0.71025$ and the Shin Etsu JNdi-1 standard $^{143}Nd/^{144}Nd = 0.512115$.

Pb isotopes were separated by anion exchange techniques with diluted HBr as an eluant. Repeated analyses of standard NBS 981 yielded average values of $^{204}Pb/^{206}Pb = 0.05897 \pm 15$, $^{207}Pb/^{206}Pb = 0.91445 \pm 80$ and $^{208}Pb/^{206}Pb = 2.16170 \pm 180$.

Whole-rock Lu–Hf isotopic analyses were conducted using a Thermo Electron Neptune multicollector (MC)-ICP-MS. The detailed procedure for sample preparation is available in Yang et al. (2007). $^{176}Hf/^{177}Hf$ measurements were normalized to $^{179}Hf/^{177}Hf = 0.7325$. Repeated analysis of the reference material, BHVO-1, used to monitor the precision, yielded an average $^{176}Hf/^{177}Hf$ ratio of 0.283105 ± 6 (2σ), in agreement with the recommended value of 0.283100 ± 3 (Weis et al. 2005).

Analytical results

Major element oxides and trace elements

All of the rocks from Units 1, 3 and 4 at Tengchong contain <1 wt% loss on ignition (LOI; Table 1 and also Appendix 6 for complete data set). In the TAS classification diagram, the Tengchong lavas range from basalt, trachybasalt, basaltic trachyandesite to trachyandesite (Fig. 4a). All of the rocks have higher Na_2O than K_2O and plot on the boundary between the high-K calc-alkaline and shoshonitic fields (Fig. 4b, c). K_2O has a well-defined positive correlation with SiO_2 (Fig. 4b).

Olivine trachybasalts and basaltic trachyandesites from Units 1 and 3 have SiO_2 contents of 48.5–55.8 wt% and total alkalis ranging from 4.9 to 7.8 wt%. They have a relatively narrow range of MgO (4.2–6.2 wt%), Al_2O_3 16.2–17.9 wt%, Fe_2O_{3T} (7.0–10.8 wt%) and TiO_2 (1.1–1.8 wt%; Table 1). On Harker diagrams, Al_2O_3, MgO, Fe_2O_{3t}, CaO and TiO_2 show moderately good negative correlations with SiO_2.

The trachyandesites of Unit 4 have relatively high SiO_2 (56.9–61.0 wt%) and in most cases, lie on the projection of fractionation trends defined by rocks of Units 1 and 3 (Fig. 4a–c). However, these rocks together with some Unit 1 lavas are significantly enriched in P_2O_5 and form a distinct trend on the Harker diagram (Fig. 5d).

Like the major oxides, trace elements of Units 1 and 3 lavas show generally linear trends with limited scatter. MgO shows a generally negative correlation with Ta and Zr (Fig. 5e, f). The rocks of Unit 4 form distinct trace element clusters having higher Rb, and Zr than the lavas of Units 1 and 3 and moderate Sr and Ta. All the lavas of Units 1, 3 and 4 display variable LREE enrichment ($La/Yb_N = 8.2–22$) and weak negative Eu anomalies ($Eu/Eu^* = 0.98–0.70$) in the chondrite-normalized REE patterns (Fig. 6a–c). In the primitive mantle-normalized trace element diagram, the rocks are characterized by enrichment of LILE and LREE and depletion of Sr and HFSE (e.g., Nb and Ta) and show negative Ti anomalies (Fig. 6d–f).

Sr–Nd–Pb–Hf isotopes

The rocks from Units 1 and 3 have approximately similar Sr–Nd–Pb–Hf isotopes (Fig. 7) with $^{87}Sr/^{86}Sr$ ratios ranging from 0.7058 to 0.7073, εNd values from −3.1 to −6.1 (Table 2), $^{206}Pb/^{204}Pb$ from 18.0 to 18.3, $^{207}Pb/^{204}Pb$ from 15.6 to 15.7 and $^{208}Pb/^{204}Pb$ from 39.0 to 39.4 (Table 3). The trachyandesites of Unit 4 have essentially constant and more radiogenic $^{87}Sr/^{86}Sr$ ratios and lower εNd values than those of the rocks of Units 1 and 3 ($^{87}Sr/^{86}Sr = \sim 0.7085$ and $\varepsilon Nd = -8.4$ to -8.7). However, the Pb isotopes are similar to those of Units 1 and 3 (Fig. 7b, c).

The isotopic signatures of rocks from Units 1 and 3 are similar to those of an EMI mantle source (Fig. 7a–c). The Pb isotopic compositions of all the rocks plot to the left of the northern hemisphere reference line (NHRL; Fig. 7c).

The rocks of Units 1 and 3 have εHf values from +4.8 to +0.8, whereas the rocks of Unit 4 have lower values, ranging from −6.2 to −6.4 (Table 2). The Nd–Hf isotope data for the Tengchong volcanic rocks are not distributed along the mantle array (Vervoort et al. 1999) but plot along the 'zircon-free sediment array', which is between the 'seawater array" and 'igneous rock array' (Bayon et al. 2009; Fig. 7d).

Discussion

Magma differentiation and crustal contamination

Magma differentiation

The chemical trends for all the rocks (Fig. 5) are generally compatible with fractionation of olivine, plagioclase, pyroxene, apatite and magnetite, the observed phases in the lavas. The chromite grains in the lavas of Units 1 and 3 likely crystallized as an early phase from magmas with

Table 1 Major and trace elements of representative lavas from Tengchong, SE Tibetan Plateau

Sample	TC-27	TC-30	TC-31	TC-32	TC-35	TC-36	TC-39	TC-41	TC-43
Units	1	1	1	1	1	1	1	1	1
Major oxides (wt%)									
SiO_2	51.68	52.47	55.53	51.88	49.29	49.87	52.61	50.01	50.16
TiO_2	1.42	1.44	1.13	1.39	1.64	1.42	1.28	1.43	1.43
Al_2O_3	16.57	16.65	16.19	16.52	17.37	17.13	16.94	17.26	17.31
Fe_2O_3	9.54	9.86	7.83	9.67	10.77	9.06	7.49	9.00	9.01
MnO	0.15	0.14	0.12	0.16	0.16	0.15	0.13	0.17	0.15
MgO	5.35	5.56	4.52	5.35	6.19	5.63	5.81	5.70	5.48
CaO	7.10	7.39	6.20	6.76	8.88	8.81	6.67	8.89	9.09
Na_2O	3.90	3.81	3.79	3.74	3.39	3.85	3.86	3.34	3.49
K_2O	2.30	2.26	2.97	2.34	1.46	2.05	3.31	1.94	1.99
P_2O_5	0.40	0.39	0.25	0.40	0.41	0.45	0.57	0.48	0.47
LOI	0.53	0.00	0.54	0.83	−0.03	0.41	0.49	0.97	0.82
Total	98.95	99.90	99.06	99.03	99.54	98.82	99.15	99.20	99.39
Mg#	0.50	0.50	0.51	0.50	0.51	0.53	0.58	0.53	0.52
Trace element (ppm)									
Sc	19.5	20.1	18.1	21.0	22.0	22.6	17.1	22.8	23.4
V	112	119	103	114	174	159	131	159	168
Cr	119	122	117	128	38	127	99	138	139
Co	27.0	28.0	24.3	28.2	37.8	28.2	24.1	29.5	30.1
Ni	40.7	51.1	39.5	42.9	45.5	55.4	78.5	60.3	58.8
Cu	20.6	22.5	23.9	22.3	34.5	37.1	19.0	33.0	35.3
Zn	121	124	99	134	120	108	87	121	112
Rb	48.2	44.5	85.7	46.1	20.2	36.8	81.0	33.3	37.3
Sr	397	412	360	396	560	649	758	689	683
Y	26.7	26.2	25.5	28.1	24.1	23.9	23.3	24.2	24.5
Zr	187	184	233	202	142	173	198	174	178
Nb	24.1	23.6	23.4	26.2	18.4	23.2	32.4	23.5	23.4
Ba	440	437	514	470	406	765	1,061	833	773
La	31.5	32.0	47.4	34.5	26.8	41.8	66.7	41.9	41.6
Ce	62.0	61.3	91.0	64.8	51.3	78.0	126.3	80.6	78.5
Pr	7.3	7.2	9.6	7.8	6.0	8.8	13.2	8.9	9.0
Nd	28.9	28.2	34.5	30.1	24.0	33.5	48.0	33.9	33.7
Sm	5.99	6.10	6.36	6.40	5.21	6.19	7.80	6.43	6.25
Eu	1.71	1.69	1.39	1.67	1.62	1.79	1.91	1.80	1.73
Gd	5.92	5.89	5.54	6.00	5.25	5.69	5.75	5.50	5.44
Tb	0.95	0.94	0.87	0.95	0.81	0.86	0.91	0.85	0.84
Dy	5.45	5.37	4.86	5.39	4.57	4.78	4.75	4.80	4.79
Ho	1.05	1.03	0.94	1.03	0.89	0.92	0.91	0.93	0.92
Er	3.02	2.99	2.83	3.05	2.64	2.77	2.73	2.78	2.77
Tm	0.41	0.40	0.39	0.41	0.35	0.36	0.36	0.37	0.38
Yb	2.62	2.59	2.54	2.77	2.34	2.43	2.44	2.52	2.43
Lu	0.38	0.38	0.37	0.40	0.33	0.36	0.36	0.36	0.35
Hf	4.62	4.53	5.51	4.82	3.46	4.20	5.07	4.10	3.95
Ta	1.39	1.36	1.39	1.34	0.95	1.26	1.89	1.31	1.23
Pb	8.82	8.97	15.32	8.78	3.94	8.61	17.0	34.6	8.3
Th	11.4	11.8	25.7	11.0	4.6	9.4	22.7	9.4	8.3
U	1.99	3.05	5.53	1.74	1.89	2.18	1.87	1.50	1.47

Table 1 continued

Sample	TC-57	TC-2	TC-5	TC-7	TC-8	TC-9	TC-11	TC-12	TC-15	TC-16
Units	1	3	3	3	3	3	3	4	4	4
Major oxides (wt%)										
SiO_2	54.55	52.47	53.04	53.34	54.59	55.80	55.02	58.75	57.13	56.89
TiO_2	1.13	1.34	1.31	1.33	1.23	1.16	1.19	1.01	1.12	1.13
Al_2O_3	16.50	17.54	17.16	17.78	16.66	16.35	16.43	16.21	16.36	16.34
Fe_2O_3	7.97	8.49	8.31	8.40	7.83	7.40	7.54	5.94	6.52	6.56
MnO	0.13	0.14	0.14	0.14	0.13	0.12	0.13	0.11	0.11	0.11
MgO	4.84	5.41	5.33	5.32	4.88	4.43	4.67	3.48	3.79	3.78
CaO	6.66	7.52	7.50	7.28	7.10	6.62	6.71	5.31	5.86	5.94
Na_2O	3.47	3.61	3.98	3.57	4.11	3.53	4.32	4.24	3.58	3.93
K_2O	2.79	2.27	2.46	2.34	2.68	2.96	3.00	3.51	3.25	3.26
P_2O_5	0.26	0.38	0.37	0.37	0.34	0.32	0.34	0.39	0.45	0.45
LOI	0.69	0.70	0.32	−0.06	0.36	0.50	0.47	0.53	0.61	0.67
Total	98.99	99.88	99.92	99.81	99.90	99.20	99.83	99.47	98.78	99.05
Mg#	0.52	0.53	0.53	0.53	0.53	0.52	0.52	0.51	0.51	0.51
Trace element (ppm)										
Sc	19.6	20.2	20.3	21.0	20.8	18.9	20.4	15.4	14.9	16.4
V	115	142	132	148	142	128	134	101	103	106
Cr	130	131	131	135	129	116	119	55	60	60
Co	26.4	28.1	28.5	29.2	27.7	25.3	26.7	17.6	18.2	18.4
Ni	44.2	59.2	59.3	61.4	60.2	53.7	54.7	52.5	57.1	54.6
Cu	25.2	23.9	29.1	25.9	30.7	27.9	31.0	22.4	22.9	19.9
Zn	122	99	102	103	110	93	97	97	101	97
Rb	78.4	37.7	49.5	47.3	78.4	94.8	86.3	119.1	96.4	96.1
Sr	397	497	497	473	476	452	459	523	550	554
Y	27.2	24.9	24.8	26.1	25.5	25.4	25.4	26.7	25.9	26.3
Zr	241	204	202	215	210	206	209	326	331	334
Nb	24.0	23.5	23.5	24.3	23.7	24.1	24.0	29.3	29.1	29.4
Ba	527	516	507	504	478	484	482	932	1,012	1,005
La	48.0	39.1	38.4	39.3	39.3	43.4	41.9	72.9	73.6	73.0
Ce	88.3	75.4	73.4	77.3	76.0	83.5	81.2	140.5	143.5	144.3
Pr	9.8	8.4	8.2	8.5	8.2	9.0	8.8	14.7	15.1	15.1
Nd	35.2	31.7	30.6	31.2	30.2	32.5	31.5	53.1	54.8	55.1
Sm	6.61	6.06	5.92	5.90	5.75	6.01	6.11	9.04	9.39	9.20
Eu	1.46	1.61	1.49	1.44	1.42	1.31	1.39	1.78	1.97	1.90
Gd	5.76	5.46	5.33	5.16	4.92	4.93	5.21	6.76	7.05	6.91
Tb	0.88	0.86	0.82	0.84	0.80	0.79	0.81	0.97	1.01	1.03
Dy	4.91	4.93	4.69	4.66	4.42	4.34	4.36	5.12	5.22	5.23
Ho	0.98	0.93	0.91	0.90	0.84	0.83	0.85	0.95	0.95	0.95
Er	2.84	2.80	2.73	2.59	2.46	2.45	2.55	2.81	2.87	2.87
Tm	0.40	0.38	0.37	0.36	0.34	0.34	0.33	0.37	0.37	0.38
Yb	2.59	2.47	2.44	2.19	2.19	2.20	2.25	2.46	2.52	2.50
Lu	0.36	0.37	0.34	0.34	0.31	0.32	0.33	0.36	0.35	0.35
Hf	5.54	4.70	4.63	4.49	4.23	4.42	4.51	7.40	8.09	8.00
Ta	1.31	1.37	1.32	1.27	1.21	1.21	1.25	1.67	1.65	1.63
Pb	14.5	12.0	11.4	10.9	11.0	12.2	11.9	23.0	21.2	21.8
Th	19.4	16.3	14.5	13.1	12.4	14.4	14.2	25.5	24.2	23.1
U	1.87	1.87	1.67	1.77	1.78	1.96	1.96	3.24	2.83	2.87

Table 1 continued

Sample	TC-19	TC-21	TC-22	TC-23	TC-26
Units	4	4	4	4	4
Major oxides (wt%)					
SiO_2	60.47	58.35	58.69	57.33	57.34
TiO_2	0.93	1.07	1.07	1.10	1.10
Al_2O_3	15.78	16.25	16.48	16.38	16.59
Fe_2O_3	5.52	6.28	6.24	6.44	6.42
MnO	0.10	0.11	0.11	0.11	0.11
MgO	3.02	3.70	3.55	3.76	3.86
CaO	4.85	5.66	5.60	5.81	5.83
Na_2O	3.73	3.80	3.54	3.95	3.85
K_2O	3.79	3.42	3.45	3.35	3.33
P_2O_5	0.36	0.43	0.43	0.45	0.45
LOI	0.60	0.42	0.28	0.28	0.37
Total	99.16	99.49	99.46	98.97	99.25
Mg#	0.49	0.51	0.50	0.51	0.52
Trace element (ppm)					
Sc	14.5	16.8	16.8	15.6	15.5
V	89	111	108	109	100
Cr	53	73	63	59	60
Co	15.7	19.5	19.2	20.3	18.0
Ni	46.5	62.8	93.2	59.0	57.2
Cu	18.3	25.2	24.6	24.7	21.6
Zn	115	123	124	153	115
Rb	138.4	111.6	111.9	98.8	96.5
Sr	467	553	555	551	550
Y	26.4	27.6	27.0	26.3	25.5
Zr	304	336	339	330	324
Nb	29.5	30.4	30.8	29.6	28.7
Ba	844	933	914	968	992
La	71.0	69.5	70.8	70.5	73.7
Ce	138.9	136.5	138.4	139.8	140.7
Pr	14.5	14.1	14.2	14.5	14.9
Nd	51.0	50.9	50.3	52.8	54.1
Sm	8.39	8.73	8.41	8.79	9.18
Eu	1.57	1.81	1.73	1.82	1.85
Gd	6.31	6.47	6.29	6.80	6.76
Tb	0.93	0.95	0.95	0.97	1.02
Dy	4.87	4.72	4.69	5.00	5.21
Ho	0.89	0.90	0.86	0.91	0.98
Er	2.68	2.56	2.49	2.68	2.86
Tm	0.35	0.34	0.34	0.36	0.38
Yb	2.27	2.17	2.10	2.36	2.46
Lu	0.34	0.31	0.32	0.33	0.37
Hf	6.54	6.86	6.67	7.56	7.86
Ta	1.74	1.47	1.44	1.49	1.67
Pb	22.2	17.8	17.3	19.7	22.6
Th	22.8	16.5	16.4	19.3	25.6
U	3.15	2.57	2.54	3.11	3.53

Fe_2O_3 as total iron. *LOI* loss on ignition

MORB-like compositions. The most magnesian olivine of the lavas at Tengchong has a composition of $Fo_{84.8}$, yielding a Mg# of 0.63 and an initial MgO/FeO ratio of 0.93 using the equation of Roeder and Emslie (1970). These values are higher than the Mg#s and MgO/FeO ratios of the olivine-bearing rocks of Units 1 and 3

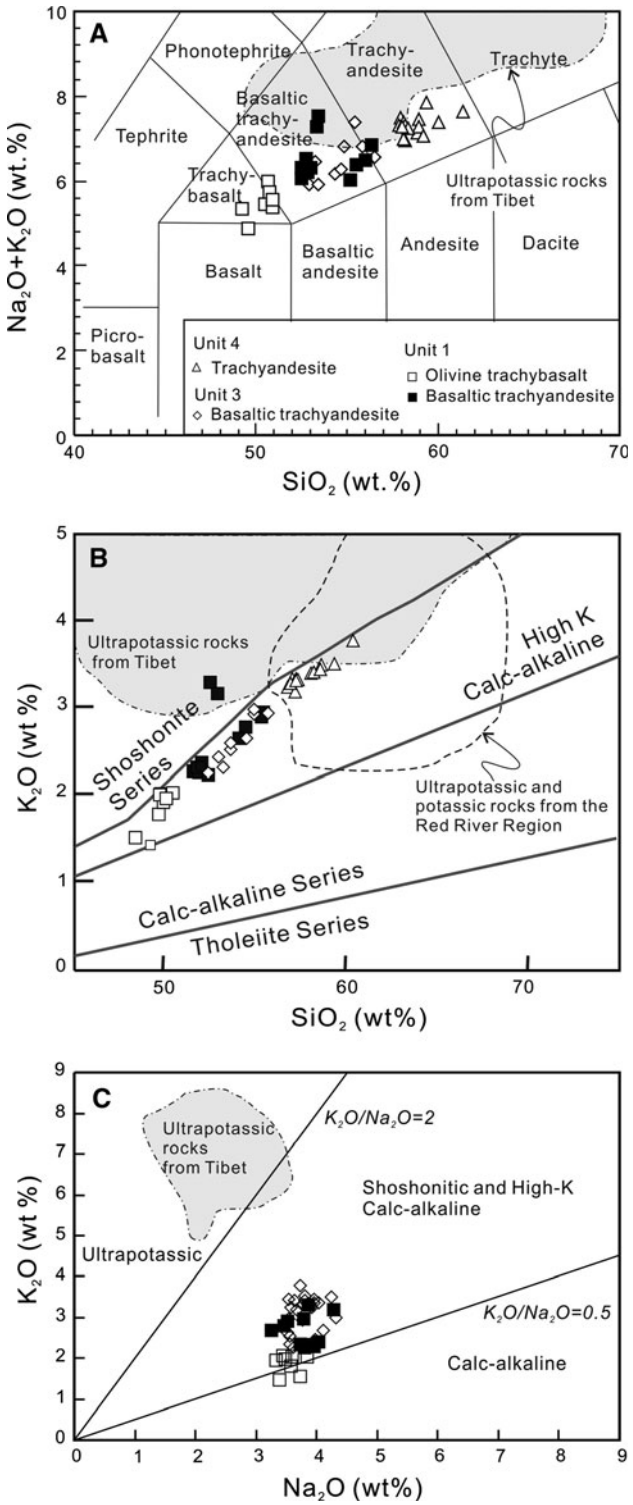

Fig. 4 Total alkali versus silica (TAS) (**a**), K_2O versus SiO_2 (**b**) and Na_2O versus K_2O (**c**) (Le Maitre et al. 1989) for lavas at Tengchong

(Table 1), suggesting significant fractional crystallization before eruption. Olivine phenocrysts in rocks of Units 1 and 3 have Fo values ranging from 84.8 to 71.2, whereas the groundmass olivine has Fo values as low as 59.2. The wide range of Fo values indicates continued crystallization during transport and eruption of the lavas.

It has been traditionally thought that all the rocks at Tengchong have continuous chemical trends and formed simply by differentiation of a single parental magma (Zhu et al. 1983; Cong et al. 1994; Wang et al. 2006). However, a close examination of the Harker diagrams (Figs. 4, 5) shows several differentiation trends. For example, in the plot of CaO versus SiO_2, rocks of Units 3 and 4 show slightly different trends (Fig. 5c). Plots of P_2O_5 versus SiO_2 reveal two parallel trends, one including some of the basaltic trachyandesites of Unit 1 and the trachyandesites of Unit 4 and the other including the trachybasalts of Unit 1 and trachyandesites of Units 1 and 3 (Fig. 6e). These trends are difficult to link by fractional crystallization of a single magma and suggest the presence of several slightly different parental magmas. Most incompatible trace elements (e.g., Ta and Zr) in the rocks of Units 1, 3 and 4 correlate negatively with MgO (Fig. 5e, f), demonstrating some assimilation-fractional crystallization (AFC) processes in their evolution.

Crustal contamination

Earlier isotopic studies suggested that the Tengchong lavas underwent very little contamination (Zhu et al. 1983; Chen et al. 2002; Zou et al. 2010), despite the presence of abundant crustal xenocrysts (Fig. 3e, f). The rocks of Units 1 and 3 are mafic in composition and have similar, relatively low $^{87}Sr/^{86}Sr$ ratios, and εNd and εHf values, indicating derivation from a common source and ruling out involvement of significant crustal material. Rocks of Unit 4 have much higher $^{87}Sr/^{86}Sr$ ratios and much lower εNd and εHf values than those of Units 1 and 3 (Table 2), and follow clear crustal contamination trends (Fig. 7b). Thus, we conclude that the rocks of Units 1 and 3 have undergone very little crustal contamination but that those of Unit 4 have been significantly modified.

Staging magma chambers

The Tengchong region is considered an active volcanic field because magma still exists at shallow levels. Active geothermal systems at Tengchong are well known (Tong and Zhang 1989; Huangpu and Jiang 2000; Du et al. 2005), and a low-velocity layer at a depth of 3–10 km, identified by seismic sounding data, and earthquake results (Qin et al. 2000; Bai et al. 2002; Zhao et al. 2006) are consistent with the presence of magma chambers in the upper crust.

Crystal fractionation recorded in the lavas at Tengchong may have occurred during and after magma emplacement into crustal chambers or on the way from the chambers to

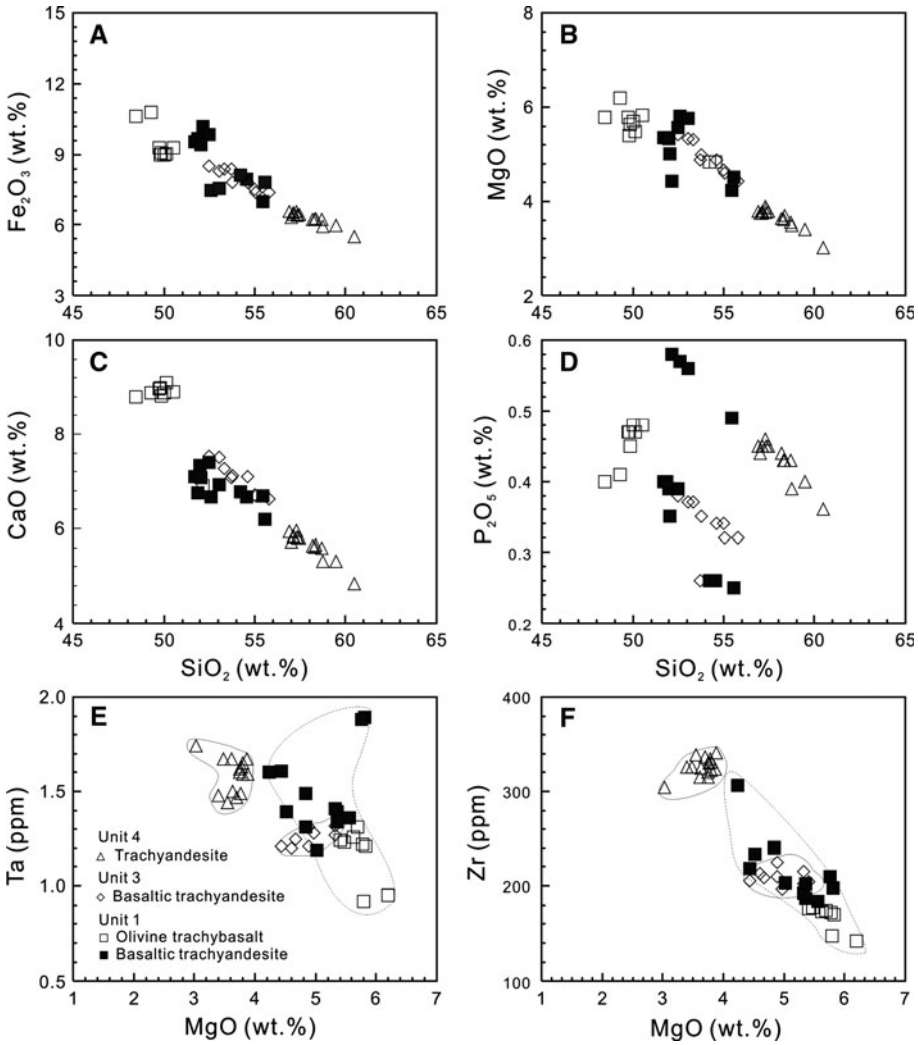

Fig. 5 Harker diagrams of SiO_2 versus Fe_2O_{3total}, MgO, CaO, P_2O_5, Ta and Zr for the lavas at Tengchong

the surface. The majority of differentiation probably took place in one or more staging magma chambers in the middle or lower crust. Slightly different chemical trends of the different lava groups can best be explained by eruption of batches of new, variably evolved and/or contaminated magma from staging chambers.

Nature of the mantle source and its heterogeneity

The source of the lavas at Tengchong would have been a MORB-like mantle as demonstrated by Cr-spinel compositions, which are similar to those of MORB (Fig. 3). Thus, we suggest that the magmas were formed at a level deeper than normal arc volcanic rocks. This difference is further reflected in the higher TiO_2 contents and Ti/V ratios of the Tengchong lavas than typical arc rocks (Table 1, Fig. 8a). In the plot of La/Nb versus Ba/Nb, the Tengchong rocks fall between the arc volcanic and Dupal OIB fields (Fig. 8b). They have higher Nb/Y ratios than arc basalts (Fig. 8c) and plot in the field of mixed asthenospheric mantle sources, having variable but lower Nb/La ratios than average oceanic island basalts (OIB; Fig. 8d).

The least contaminated lavas from Units 1 and 3 are enriched in LREE (Fig. 6a, b), consistent with a garnet-bearing mantle source (c.f. van Westrenen et al. 2000). Rocks from Unit 1 have higher Sr/Y ratios (>15) than normal arc rocks, consistent with melting at the garnet stable depth. The lavas at Tengchong have Sm/Yb ratios higher than the spinel lherzolite melting curve, but lower than the garnet-lherzolite melting trend (Fig. 9a). The rocks all plot near the garnet + spinel lherzolite mantle source in the Sm/Yb versus La/Sm diagram (Fig. 9b).

The mantle source may have been heterogeneous, because the rocks of Units 1 and 3 showing the least crustal contamination have variable isotopic compositions (Fig. 7). They show two different trends in particular in the plot of SiO_2 versus P_2O_5 (Fig. 5d). They also have different Nb/Y, La/Yb and Nb/La ratios (Fig. 8c, d), clearly reflecting variable compositions of the mantle sources because these elements have similar partition coefficients during mantle melting and fractionation.

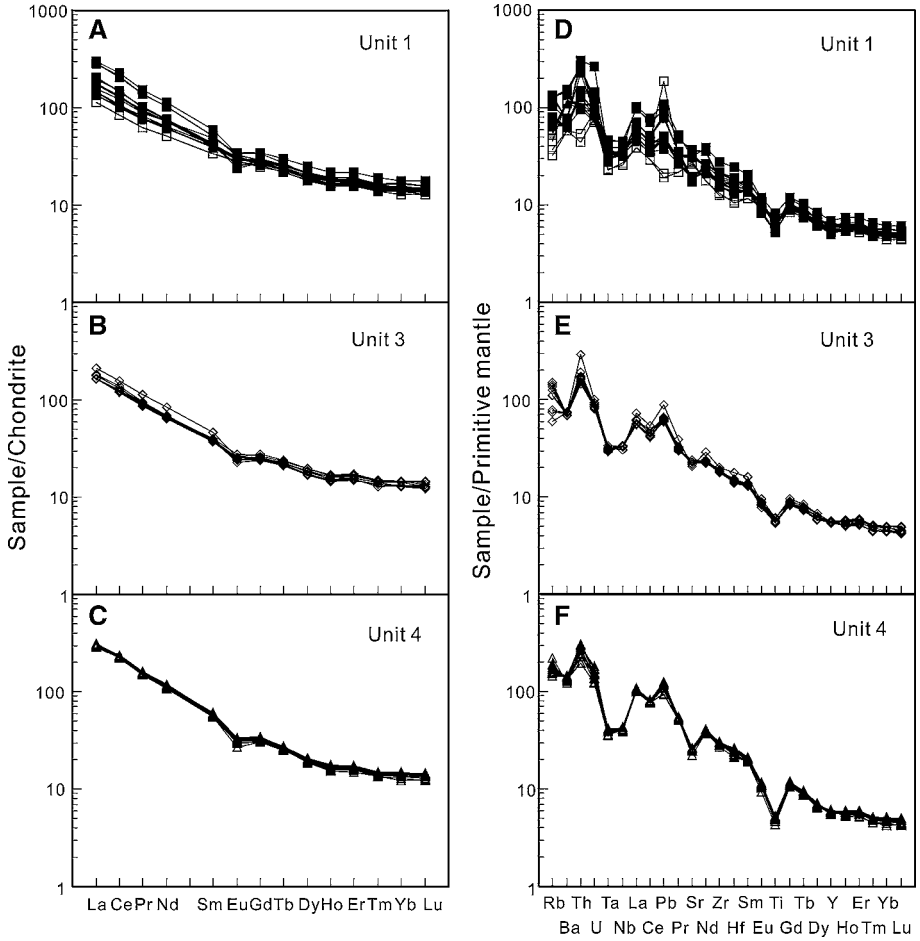

Fig. 6 Chondrite-normalized REE patterns (**a–c**) and primitive mantle-normalized trace element patterns (**d–f**) for the lavas at Tengchong. Normalization values after Sun and McDonough (1989)

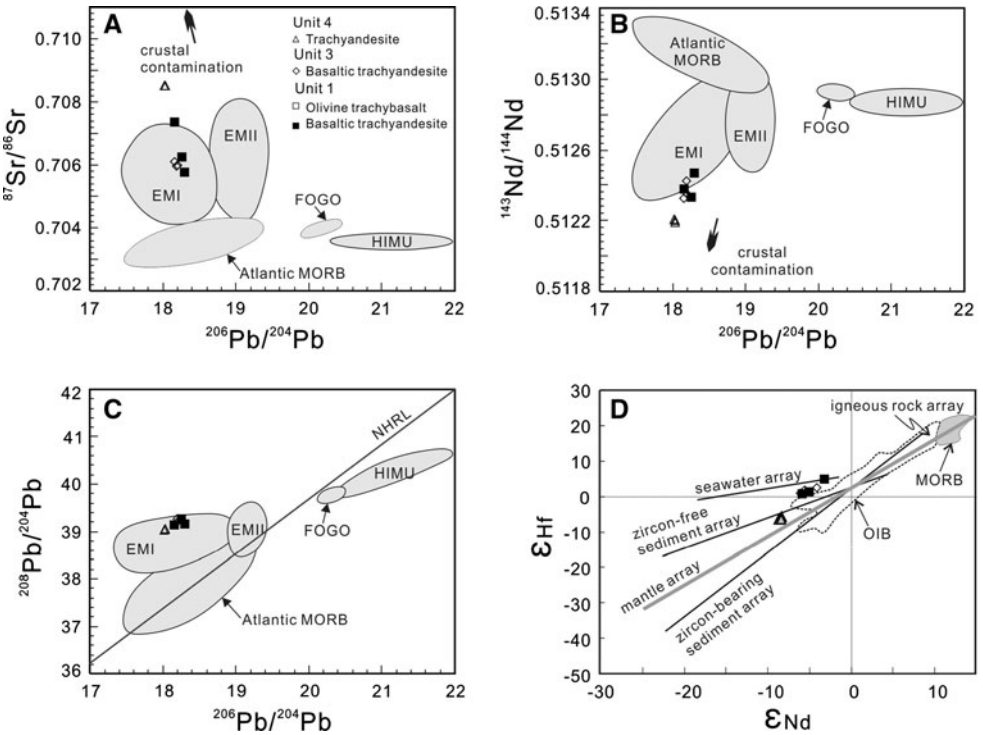

Fig. 7 Plots of Sr–Nd-Pd-Hf isotopic compositions for the lavas at Tengchong. **a** $^{206}Pb/^{204}Pb$ versus $^{87}Sr/^{86}Sr(t)$; **b** $^{206}Pb/^{204}Pb$ versus initial $^{143}Nd/^{144}Nd$; **c** $^{206}Pb/^{204}Pb$ versus $^{208}Pb/^{204}Pb$; and **d** εHf versus εNd. Data sources: reference fields in **a–c** are from Zindler and Hart (1986), Hart (1988) and Hart and Zindler (1989); Reference fields for MORB and OIB in **d** are after Vervoort et al. (1999). The mantle array (εHf = 1.33; εNd + 3.19) is adapted from Vervoort et al. (1999) and the igneous rock array (εHf = 1.37; εNd + 2.89) from Bayon et al. (2009)

Table 2 Sr–Nd–Hf isotopes of representative lavas from Tengchong, SE Tibetan Plateau

Sample	Unit	Rb (ppm)	Sr (ppm)	$^{87}Rb/^{86}Sr$	$^{87}Sr/^{86}Sr$	$2\sigma_m$	Sm (ppm)	Nd (ppm)	$^{147}Sm/^{144}Nd$
TC32	1	45.6	403	0.3266	0.705806	13	6.18	30.2	0.1238
TC39	1	84.6	778	0.3145	0.707362	14	7.53	47.4	0.0961
TC58	1	66.9	399	0.4854	0.706275	11	6.19	34.2	0.1095
TC5	3	49.4	500	0.2859	0.705977	12	5.75	30.6	0.1136
TC8	3	74.8	462	0.4681	0.706018	15	5.63	30.7	0.1108
TC10	3	85.2	442	0.5580	0.706118	11	5.75	31.9	0.1087
TC13	4	108	530	0.5876	0.708515	12	8.73	53.5	0.0986
TC16	4	97.1	563	0.4987	0.708513	13	8.78	53.7	0.0989
TC22	4	107	530	0.5817	0.708509	12	8.63	53.1	0.0983

Sample	Unit	$^{143}Nd/^{144}Nd$	$2\sigma_m$	εNd	Lu (ppm)	Hf (ppm)	$^{176}Lu/^{177}Hf$	$^{176}Hf/^{177}Hf$	$2\sigma_m$	εHf
TC32	1	0.512476	12	−3.2	0.39	4.78	0.0116	0.282908	10	4.8
TC39	1	0.512379	14	−5.1	0.34	4.99	0.0097	0.282806	7	1.3
TC58	1	0.512337	11	−5.9	0.38	5.63	0.0096	0.282795	6	0.9
TC5	3	0.512428	14	−4.1	0.37	4.65	0.0113	0.282842	3	2.5
TC8	3	0.512353	13	−5.6	0.37	4.79	0.0109	0.282820	6	1.8
TC10	3	0.512326	11	−6.1	0.34	4.69	0.0103	0.282801	6	1.1
TC13	4	0.512192	10	−8.7	0.35	7.45	0.0067	0.282592	4	−6.3
TC16	4	0.512208	13	−8.4	0.36	7.66	0.0066	0.282587	6	−6.4
TC22	4	0.512204	15	−8.5	0.35	7.44	0.0068	0.282594	5	−6.2

Table 3 Pb isotopic data of representative lavas from Tengchong, SE Tibetan Plateau

Unit	Sample	$^{206}Pb/^{204}Pb$	$\pm2\sigma$	$^{207}Pb/^{204}Pb$	$\pm2\sigma$	$^{208}Pb/^{204}Pb$	$\pm2\sigma$
1	TC32	18.30	0.01	15.68	0.01	39.17	0.01
1	TC39	18.16	0.02	15.69	0.03	39.14	0.03
1	TC58	18.25	0.01	15.71	0.02	39.27	0.02
3	TC5	18.19	0.03	15.69	0.03	39.18	0.03
3	TC8	18.20	0.02	15.71	0.02	39.27	0.03
3	TC10	18.16	0.01	15.67	0.01	39.15	0.01
4	TC13	18.03	0.02	15.65	0.02	39.06	0.02
4	TC16	18.02	0.02	15.64	0.02	39.04	0.02
4	TC22	18.03	0.02	15.65	0.03	39.06	0.04

We conclude that the rocks at Tengchong were generated from a mantle source that was isotopically and chemically heterogeneous due to various degrees of enrichment of LREE and depletion of HFSE (Ti, Nb and Ta; c.f. Arndt et al. 1998). Melting of this highly heterogeneous mantle produced a range of primary magmas, which were injected into shallower staging magma chambers where they experienced variable fractionation and crustal assimilation before final eruption.

Subduction-modified mantle source

Lavas at Tengchong have an arc-like geochemical affinity with an EMI-like mantle source as demonstrated by their isotopic compositions (Fig. 9). Such a source is traditionally explained to be subduction-related and likely modified by slab-related fluids and crustal materials (Alabaster et al. 1982). Because Sr is more compatible than Ce in phlogopite (LaTourrette et al. 1995), the negative correlation between Sr/Ce and Th in the Tengchong lavas (Fig. 9c) may reflect the presence of phlogopite in the mantle (c.f. Yang et al. 2003) due to fluid-related metasomatism. Such a fluid would likely have been derived from subducted altered oceanic crust and associated sediments.

The enrichment of Th over LREE and LILE provides a possible key to the origin of these rocks and their mantle source. The abundance of highly incompatible elements (LILE, e.g., Rb, Sr and Ba) in magma sources is generally

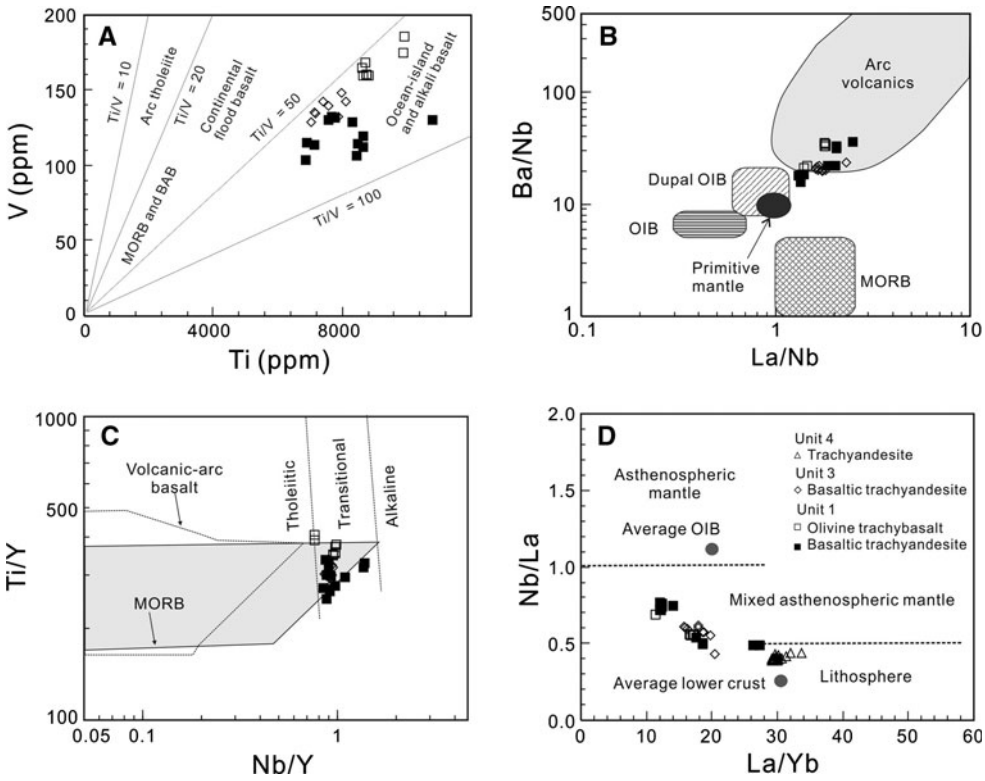

Fig. 8 Plots of elements and elemental ratios for the lavas at Tengchong: **a** Ti versus V (after Shervais 1982); **b** Nb/Y versus Ti/Y (Pearce 1982); **c** La/Yb versus Nb/La (after Watson 1993); and **d** La/Nb versus Ba/Nb (after Jahn et al. 1999) with data sources: *PM* primitive mantle (Sun and McDonough 1989); *CC* average continental crust (Taylor and McLennan 1985; Condie 1993); Clastic sediment average (Condie 1993); MORB, OIB and Dupal OIB (Le Roux 1986)

controlled by fluid influx (Stolper and Newman 1994). Compared to LILE, Th and HFSE (Zr, Hf, Nb and Ta) are relatively immobile in aqueous fluids (Tatsumi 1986). Therefore, enrichment of LILE and LREE is indicative of involvement of slab fluids, whereas enrichment of REE and HFSE in a mantle wedge indicates an introduction of slab melts (Elliott et al. 1997; Plank and Langmuir 1998). Although high Th/Ba and Th/La ratios of the lavas at Tengchong clearly point to melt-related enrichment (Fig. 9c), relatively low $(Th/Ba)_N$ and $(Th/La)_N$ ratios of olivine trachybasalts of Unit 1 may indicate that the source was modified by slab-derived fluids.

LILE enrichment can be examined using a plot of Th/Yb versus Ta/Yb, where Yb-normalization is used to eliminate the effects of partial melting and fractional crystallization (Pearce 1982). Melt-related enrichment processes affect Th and Ta equally because of similar partition coefficients during mantle melting and would produce magmas which lie along the "within-plate" trend in the plot. However, lavas at Tengchong all plot above the "within-plate" array with much higher Th/Yb ratios, even higher than many subduction-related rocks (Fig. 9e). This selective enrichment of Th can be best explained by greater mobility of LILE in hydrous fluids relative to HREE and HFSE.

Hydrous fluids from subducted slabs can be derived either from altered oceanic crust (AOC) or from subducted sediments, and these sources can be clearly distinguished in plots of Ba/Zr versus Th/Zr (Ishizuka et al. 2003). The lavas at Tengchong have high Ba/Zr and Th/Zr ratios relatively to Pacific Ocean and Philippine Sea MORB and clearly plot between the fields of AOC fluids and bulk sediment (Fig. 9f), confirming that large amounts of fluid from altered oceanic crust and sediment were added to the mantle source. Melt-related enrichment of the source region is also demonstrated in Fig. 9g, h.

The high $^{208}Pb/^{204}Pb$ ratios of the lavas at Tengchong relative to MORB support involvement of a sediment component in the genesis of these rocks. The interpretation of a mantle source modified by sediment-derived Pb is favored over the introduction of radiogenic Pb into the ascending magma at upper-crustal levels, because of the similar Pb isotopes of the three units. They have relatively high εHf and εNd values and therefore plot above the igneous rock array, lying between the seawater and zircon-free sediment arrays (Fig. 7d), suggesting that the sediment component in the source regions was mud rather than sand (Chauvel and Blichert-Toft 2001; Eisele et al. 2002; Chauvel et al. 2008).

An integrated model for the Tengchong volcanoes

The lavas at Tengchong have relatively high K_2O, plotting in the field of K-rich calc-alkaline lavas and shoshonites (Fig. 4b), but are distinctly different from the post-collisional potassic and ultrapotassic volcanic rocks in Tibet that were generated by subduction of continental crust. Although they have an affinity to rocks produced by active

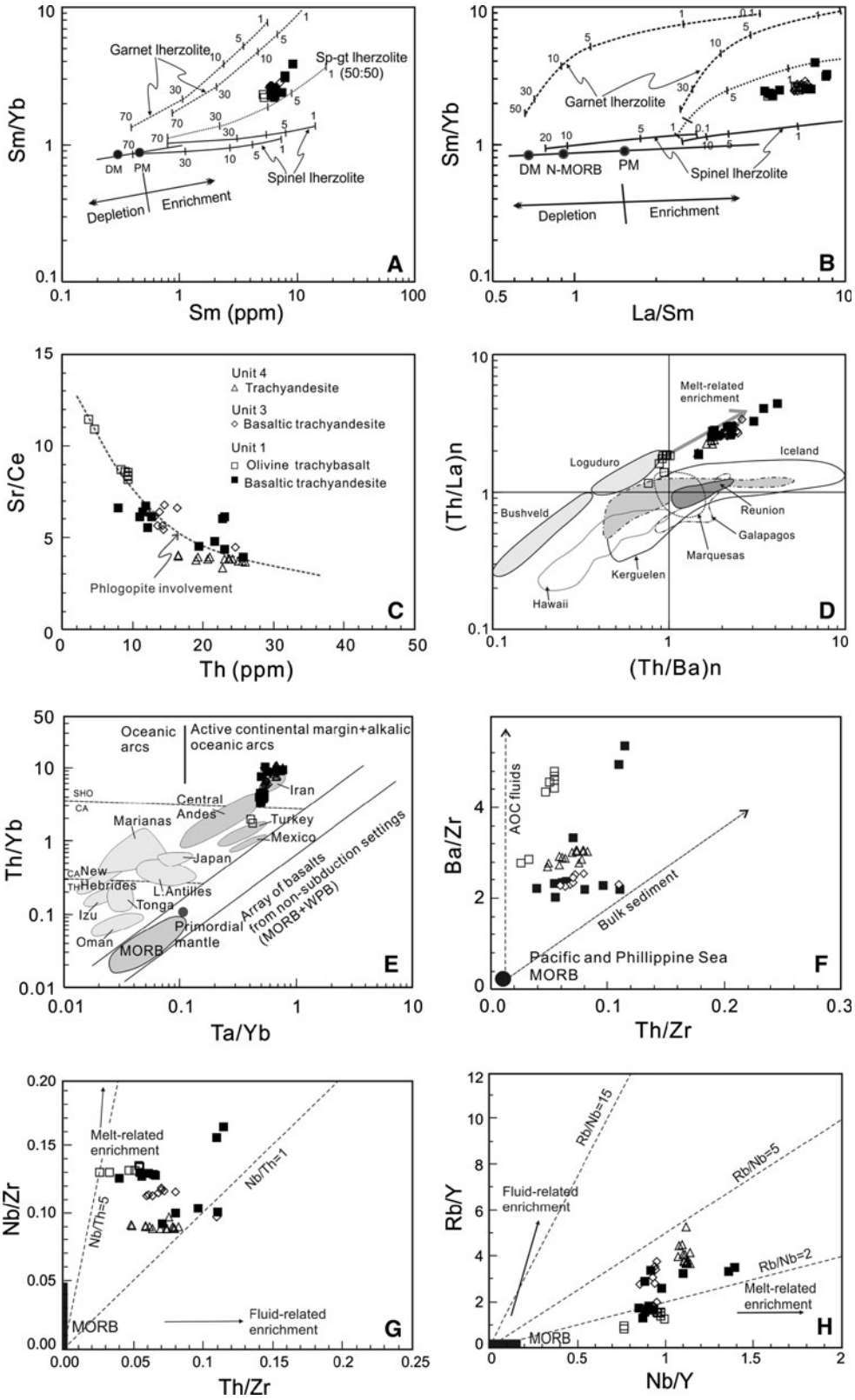

Fig. 9 Plots of **a** Sm/Yb versus Sm and **b** Sm/Yb versus La/Sm for the lavas at Tengchong. Mantle array (*heavy line*) defined by depleted MORB mantle (DMM, McKenzie and O'Nions 1991) and primitive mantle (PM, Sun and McDonough 1989). Melting curves for spinel lherzolite (Ol53 + Opx27 + Cpx17 +Sp11) and garnet peridotite (Ol60 + Opx20 + Cpx10 +Gt10) with both DMM and PM compositions are after Aldanmaz et al. (2000). *Numbers along lines* represent the degree of the partial melting. **c** Sr/Ce versus Th showing a negative correlation; **d** Th/Ba versus Th/La (after Gasperini et al. 2000); **e** Th/Yb versus Ta/Yb (Pearce 1983); **f** Ba/Zr versus Th/Zr, the *dashed arrow line* is the mixing line between the mantle wedge and AOC fluid, and the *solid arrow line* is the mixing trend between the mantle wedge and bulk sediment (Ishizuka et al. 2003); **g** Th/Zr versus Nb/Zr; and **h** Nb/Y versus Rb/Y. Reference fields in both **d** and **e** are from Kepezhinskas et al. (1997)

subduction, their TiO_2 and Nb contents are higher than those of typical intra-oceanic arc basalts ($TiO_2 < 1$wt% and Nb < 2 ppm) and of subduction-related calc-alkaline andesites. Their high TiO_2 and P_2O_5 contents are more comparable to ocean island lavas. Thus, the unusual compositions indicate derivation from a variably modified mantle source.

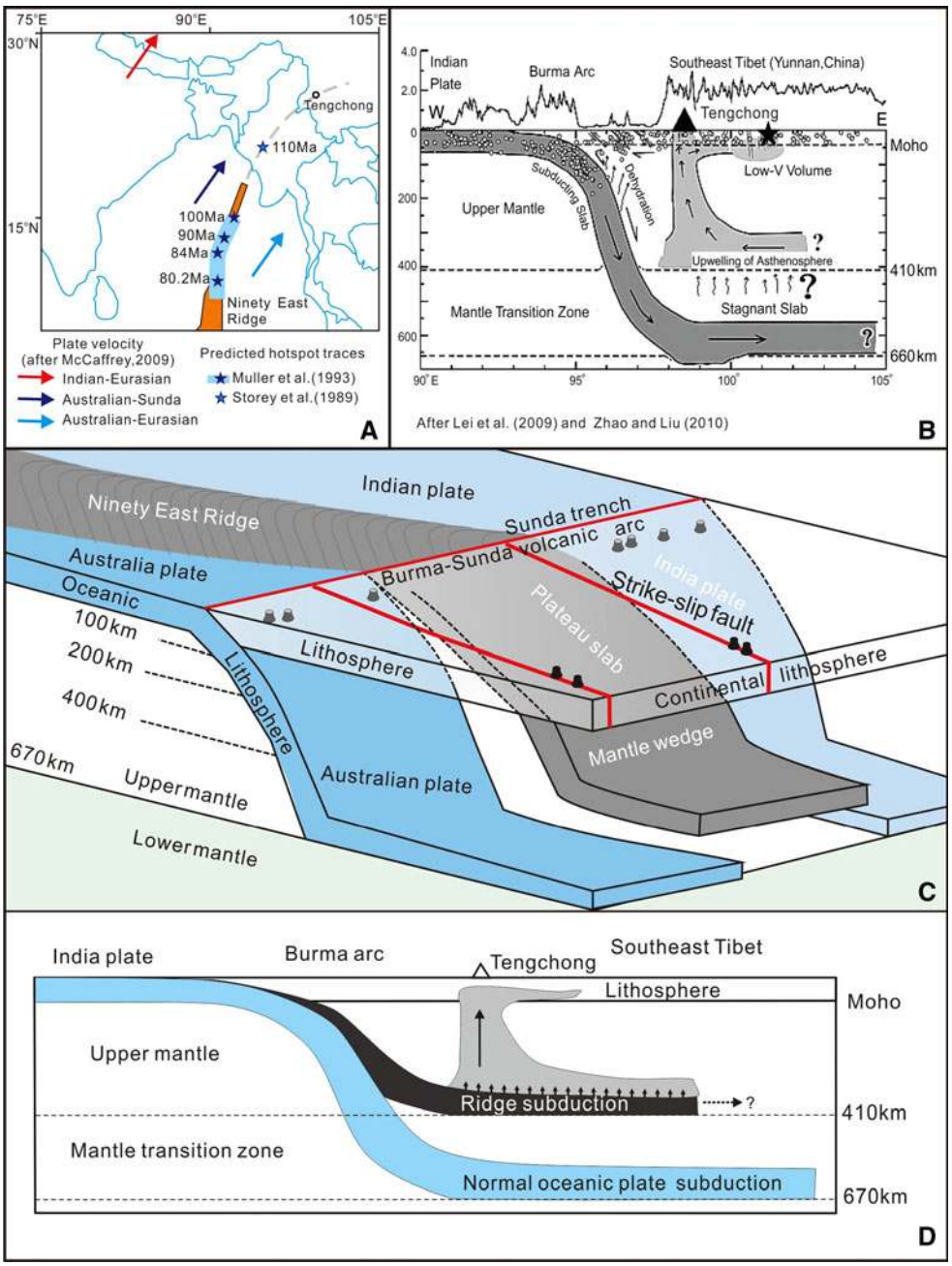

Fig. 10 **a** Plate tectonic setting of SE Asia (After McCaffrey 2009). The Ninety East Ridge is marked by volcanic rocks related to the Kerguelen hotspot (Seno and Rehman 2011). The hotspot traces on the Indian plate over the Kerguelen hotspots younger than 100 Ma are from Muller et al. (1993) and are shown by the *blue lines* with ages; it is noted that the traces of 110 Ma are from Storey et al. (1989); **b** Interpretation of P-wave tomography passing through the Tengchong volcanic field (After Zhao and Liu 2010). **c** A schematic diagram showing the subduction of the buoyant Ninety East Ridge. **d** New interpretation of the geophysical data

The Mali-Hka Mandalay suture zone west of Tengchong contains ophiolites like those of the Yarlung-Zangbo suture in Tibet and the two are thought to be part of the same zone, marked by subduction of Neo-Tethyan oceanic subduction prior to the collision of India and Eurasia (Fig. 1). Subduction of Neo-Tethyan lithosphere produced the Gangdese arc rocks, such as the 70–40 Ma Linzizong volcanic succession (Chung et al. 2005, Mo et al. 2007), and the Mesozoic granitoids in the Tengchong area. Closure of the Neo-Tethyan Ocean at either Late Cretaceous (~65 Ma) or Oligocene (~34 Ma; Yin and Harrison 2000; Aitchison et al. 2007) was followed by subduction of Indian continental crust beneath Eurasia. In the Gaoligong area, north of Tengchong, ~40-Ma mafic dykes and lavas are thought to be related to slab break-off in the early stages of continental collision and thus record the final closure of the ocean (Xu et al. 2008, Gao et al. 2010).

Post-collisional magmatism associated with this subduction generated the potassic and ultrapotassic volcanic rocks of the Tibetan Plateau (Mo et al. 2006; Zhao et al. 2009). Potassic and ultrapotassic rocks along the Red River Fault show Sr–Nd isotopic compositions similar to those of the Indian continental basement, providing evidence for subduction of the Indian continental crust underneath Tibet and SW China (Wang et al. 2001; Zhao et al. 2003; Guo et al. 2006). Seismological data indicate the presence of a modern,

eastward-dipping zone of earthquake foci beneath the Burma Central Lowlands (Huan et al. 1981; Lei et al. 2009).

In contrast to other parts of the Tibetan Plateau, subduction of the Indian continental crust beneath Burma and SW China was later replaced by the subduction of the Indian Oceanic plate. This plate continues to move northward and is currently being subducted beneath Burma and SW China (Fig. 10a). A hydrous zone under Tengchong, defined by geophysical data (Bai et al. 2002), likely reflects dewatering of this slab. High-resolution P-wave tomography of the Tengchong region indicates a broad low-velocity zone about 100 km wide that extends down to the 410-km discontinuity (Lei et al. 2009; Zhao and Liu 2010). The modern volcanism at Tengchong was recently explained to be probably related to deep subduction of the Indian Ocean plate along a discontinuity at ~660 km (Zhao and Liu 2010; Fig. 10b). However, the oceanic slab at this depth would have already dehydrated so that it cannot explain the low-velocity zone at the 410-km discontinuity described by Zhao and Liu (2010). This portion of the Indian Ocean plate contains the northern end of the Ninety East Ridge (Figs. 1, 10a). This ridge was formed by eruptions from the Kerguelen hotspot during the last 130 million years (Muller et al. 1993) and drifted northward and then northeastward near the Tengchong region at 110 Ma (Storey et al. 1989). Thus, an older portion of the Indian Ocean crust and the Ninety East Ridge is likely somewhere beneath the Tengchong area. The plateau ridge would be more buoyant than the adjacent normal oceanic lithosphere, causing a kink, or tear, in the downgoing slab, for a much flatter subduction (Fig. 10c). Therefore, we propose that the volcanism in Tengchong was due to the much flatter Ninety East Ridge subduction likely along the ~410 km discontinuity (Fig. 10d).

The present-day ocean plate subduction was preceded by subduction of Indian continental crust, which presumably added a continental component to the source region that was responsible for the evolved isotopic compositions observed in the lavas. This modification by the Indian continental crust may also have produced the K_2O enrichment of the lavas at Tengchong. The ridge has an OIB component (Storey et al. 1989) which could explain some of unusual features of the Tengchong lavas, including the OIB and arc characteristics of the lavas. The OIB-type volcanic rocks of the ridge may be more resistant to melting during subduction than MORB, thus metasomatizing the mantle wedge at a depth deeper than the source required for normal arc volcanoes. The ridge subduction would have brought altered basalts, water and sediment to the wedge to form a heterogeneous mantle source.

Thus, the unusual compositions of the lavas at Tengchong reflect long-lived and repeated modification of the mantle source by subduction of oceanic and continental lithosphere. The generation and eruption of the magmas are likely linked to transtensional faulting in the region. Both the Tengchong and Wuntho volcanic fields lie along major, right-lateral, transtensional faults, which are known to extend into the lower crust and probably the upper mantle (Qin et al. 2000). Movement on these two faults may have produced local extension, increased crustal permeability and enhanced the delivery of mantle-derived melts to the overlying crust to allow magma accumulation and eruption.

Conclusions

Lavas at Tengchong include olivine trachybasalt, basaltic trachyandesite, trachyandesite and hornblende dacite, typical of an arc-like assemblage. However, they are unique in terms of their high TiO_2 and P_2O_5 contents and extremely high Th relative to typical arc volcanic rocks. Olivine trachybasaltic and trachyandesitic rocks were derived from variably differentiated magmas, but their compositions were primarily controlled by a heterogeneous mantle source and variable degrees of crustal contamination. The mantle source was metasomatized by the subduction of the earlier Indian continental crust and then the Indian Oceanic plate, probably the Ninety East Ridge. The current modification was produced by the introduction of slab fluids and melts from the subducted ridge. Strike-slip faulting may have initiated the present-day magmatism and facilitated the upward transport of mantle-derived melts. Subsequent processes controlled the compositional variations within individual lava units. These include minor contamination by continental crust and variable degrees of silicate and oxide fractionation in staging magma chambers.

Acknowledgments Support from research grants from the State Key Laboratory of Ore Deposit Geochemistry, Institute of Geochemistry, Chinese Academy of Sciences (200802) to MFZ, National Natural Science Foundation of China (41172191) to DPY, CAS Hundred Talents projects to CYW, and a CAS/SAFEA International Partnership Program for Creative Research Teams (KZCX2-YW-t004), are gratefully acknowledged. Field assistance was provided by Xu Zhangbao from the Yunnan Geological Survey. We thank two anonymous referees for helpful reviews.

References

Aitchison JC, Ali JR, Davis AM (2007) When and where did Indian and Asian collide? J Geophys Res 112. doi:10.1029/2006JB004706

Alabaster T, Pearce JA, Malpas J (1982) The volcanic stratigraphy and petrogenesis of the Oman ophiolite complex. Contrib Mineral Petrol 81:168–183

Aldanmaz E, Pearce JA, Thirlwall MF, Mitchell JG (2000) Petrogenetic evolution of late Cenozoic, post-collision volcanism in western Anatolia, Turkey. J Volcanol Geotherm Res 102:67–95

Anderson J (1871) A report on the expedition to western Yunnan via Bhamo. Calcutta

Anderson J (1876) Mandakay to Momien: a narrative of the two expeditions to west China of 1868 and 1875. Report, London

Arndt NT, Chauvel C, Czamanske G, Fedorenko V (1998) Two mantle sources, two plumbing systems: Tholeiitic and alkaline magmatism of the Maynecha River basin, Siberian flood volcanic province. Contrib Mineral Petrol 133:297–313

Bai D, Meju MA, Liao Z (2002) Magnetotelluric images of deep crustal structure of the Rehai geothermal field near Tengchong, southern China. Geophys J Int 148:1–16

Bayon G, Burton KW, Soulet G, Vigier N, Dennielou B, Etoubleau J, Ponzevera E, German CR, Nesbitt RW (2009) Hf and Nd isotopes in marine sediments: Constraints on global silicate weathering. Earth Planet Sci Lett 277:318–326

Brown JC (1913) Contributions to the geology of the province of Yunnan in the western China (1): the Bhamo-Tengyueh area. Rec Geol Surv India XLIII(3):173–205

Chang CY (1948) Extinct volcanoes of Tengchong, West Yunnan. Sci Rep Nat Tsing Hua Univ Ser C Geol Geograph Metrol Sci 1(4):291–304

Chauvel C, Blichert-Toft J (2001) A hafnium isotope and trace element perspective on melting of the depleted mantle. Earth Planet Sci Lett 190:137–151

Chauvel C, Lewin E, Carpentier M, Arndt NT, Marini JC (2008) Role of recycled oceanic basalt and sediment in generating the Hf–Nd mantle array. Nat Geosci 1:64–67

Chen F, Satir M, Ji J, Zhong D (2002) Nd–Sr–Pb isotopes of Tengchong Cenozoic volcanic rocks from western Yunnan, China: evidence for an enriched mantle source. J Asian Earth Sci 21:39–45

Chung SL, Chu MF, Zhang YQ, Xie YW, Lo CH, Lee T, Lan CY, Li XH, Zhang Q, Wang YZ (2005) Tibetan tectonic evolution inferred from spatial and temporal variations in post-collisional magmatism. Earth Sci Rev 68:173–196

Condie K (1993) Chemical composition and evolution of the upper continental crust: Contrasting results from surface samples and shales. Chem Geol 104:1–37

Cong BL, Chen QY, Zhang RY, Wu GY, Xu P (1994) Genesis of Tengchong volcanics, China. Sci China Ser D 24:441–448

Ding L, Kapp P, Yin A, Deng WM, Zhong DL (2003) Early Tertiary volcanism in the Qiangtang terrane of central Tibet: evidence for a transition from oceanic to continental subduction. J Petrol 44:1833–1865

Du JG, Liu CQ, Fu BH, Ninomiya Y, Zhang YL, Wang CW, Wang HL, Sun ZG (2005) Variations of geothermometry and chemical-isotopic compositions of hot spring fluids in the Rehai geothermal field, southwestern China. J Volcanol Geotherm Res 142:243–261

Eisele J, Sharma M, Galer SJG, Blichert-Toft J, Devey CW, Hofmann AW (2002) The role of sediment recycling in EM-1 inferred from Os, Pb, Hf, Nd, Sr isotope and trace element systematics of the Pitcairn hotspot. Earth Planet Sci Lett 196:197–212

Elliott T, Plank T, Zindler A, White W, Bourdon B (1997) Elemental transport from slab to volcanic front at the Mariana arc. J Geophys Res 102:14991–15019

Gao YF, Yang Z, Santosh M, Hou Z, Wei R, Tian S (2010) Adakitic rocks from slab melt-modified mantle sources in the continental collision zone of southern Tibet. Lithos 119:651–663

Gasperini D, Blichert-Toft J, Bosch D, Del Moro A, Macera P, Telouk P, Albarede F (2000) Evidence from Sardinian basalt geochemistry for recycling of plume heads Into the Earth's mantle. Nature 408:701–704

Guo Z, Wilson M, Liu J, Mao Q (2006) Post-collisional, potassic and ultrapotassic magmatism of the northern Tibetan Plateau: constraints on characteristics of the mantle source, geodynamic setting and uplift Mechanisms. J Petrol 47:1177–1220

Hart SR (1988) Heterogeneous mantle domains: signature, genesis and mixng chronologies. Earth Planet Sci Lett 90:273–296

Hart SR, Zindler A (1989) Constraints on the nature and development of chemical heterogeneities in the mantle. In: Peltier WD (ed) Mantle convection, plate tectonics and global dynamics, vol 4. Gordon & Breach Science Publishers, pp 261–387

Huan WL, Wang SY, Shi SL, Yan JQ (1981) The distribution of earthquake foci tectonics on the Tibetan plateau and its vicinity. In: Proceedings of the symposium on Tibetan Plateau, vol 1. Gordon and Breach, New York, pp 651–659

Huangpu G, Jiang CS (2000) Study on Tengchong volcanic activity (in Chinese with English abstract). Yunnan Technol Press, Kunming, pp 18–76

Ishizuka O, Rex N, Taylor J, Milton A, Nesbitt RW (2003) Fluid-mantle interaction in an intra-oceanic arc: constraints from high-precision Pb isotopes. Earth Planet Sci Lett 211:221–236

Jahn BM, Wu FY, Lo CH, Tsai CH (1999) Crust–mantle interaction induced by deep subduction of the continental crust: geochemical and Sr–Nd isotopic evidence from post-collisional mafic–ultramafic intrusions of the northern Dabie complex, central China. Chem Geol 157:119–146

Kamenetsky VS, Crawford AJ, Meffre S (2001) Factors controlling chemistry of magmatic spinel: an empirical study of associated olivine, Cr-spinel and melt inclusions from primitive rocks. J Petrol 42:655–671

Kepezhinskas P, McDermott F, Defant M, Hochstaedter A, Drummond MS, Hawdesworth CJ, Koloskov A, Maury RC, Bellon H (1997) Trace element and Sr–Nd–Pb isotopic constraints on a three-component model of Kamchatka Arc petrogenesis. Geochim Cosmochim Acta 61:577–600

LaTourrette TZ, Hervig RL, Holloway JR (1995) Trace element partitioning between amphibole, phlogopite, and basanite melt. Earth Planet Sci Lett 135:13–30

Le Maitre RW, Bateman P, Dudek A, Keller J, Lameyre J, Le Bas MJ, Sabine PA, Schmid R, Sorensen H, Streckeisen A, Woolley AR, Zanettin B (1989) A classification of igneous rocks and glossary of terms. Blackwell, Oxford

Le Roux AP (1986) Geochemical correlation between southern African kimberlites and south Atlantic hotspots. Nature 324:243–245

Lei JS, Zhao DP, Su YJ (2009) Insight into the origin of the Tengchong intraplate volcano and seismotectonics in southwest China from local and teleseismic data. J Geophys Res 114:B05302. doi:10.1029/2008JB005881

Li DM, Li Q, Chen WJ (2000) Volcanic activity of Tengchong since the Pliocene (in Chinese with English abstract). Acta Petrologica Sinica 16:362–370

Liu JQ (1999) Volcanoes of China. Science Press, Beijing

McCaffrey R (2009) The tectonic framework of the Sumatran subduction zone. Ann Rev Earth Plan Sci 37:345–366

McKenzie D, O'Nions RK (1991) Partial melt distribution from inversion of rare earth element concentrations. J Petrol 32:1021–1091

Mo X, Zhao Z, Deng J, Flower MF, Yu X, Luo Z, Li Y, Zhou S, Dong G, Zhu D, Wang L (2006) Petrology and geochemistry of post-collisional volcanic rocks from the Tibetan Plateau: implications for lithosphere heterogeneity and collisioninduced asthenospheric mantle flow. In: Dilek Y, Pavlides S (eds) Postcollisional tectonics and magmatism in the Mediterranean Region and Asia, vol 409. Geological Society of America Special Paper, pp 507–530

Mo XX, Hou ZQ, Niu YL, Dong GC, Qu XM, Zhao ZD, Yang ZM (2007) Mantle contribution to crustal thickening during

continental collision: evidence from Cenozoic igneous rocks in southern Tibet. Lithos 96:225–242
Mu ZG, Tong W, Curtis GH (1987a) Times of volcanic activity and origin of magma in Tengchong geothermal area, west Yunnan province (in Chinese with English abstract). Acta Geophysics Sinica 30:261–270
Mu ZG, Curtis GH, Liao Z, Wei T (1987b) K-Ar age and strontium isotopic composition of the Tengchong volcanic rocks, West Yunnan province, China. Geothermics 16:283–297
Muller RD, Royer J-Y, Lawver LA (1993) Revised plate motions relative to the hotspots from combined Atlantic and Indian Ocean hotspot tracks. Geology 21:275–278
Nomade S, Renne PR, Mo X, Zhao Z, Zhou S (2004) Miocene volcanism in the Lhasa block, Tibet: spatial trends and geodynamic implications. Earth Planet Sci Lett 221:227–243
Pearce JA (1982) Trace element characteristics of lavas from destructive plate boundaries. In: Thorpe RS (ed) Andesites: orogenic andesites and related rocks. Wiley, Chichester, pp 525–548
Pearce JA (1983) Role of the sub-continental lithosphere in magma genesis at active continental margins. In: Hawkesworth CJ, Norry MJ (eds) Continental basalt and mantle xenoliths. Shiva, Nantwich, pp 230–249
Plank T, Langmuir CH (1998) The chemical composition of subducting diment and its consequences for the crust and mantle. Chem Geol 145:325–394
Qin JZ, Huang PG, Li Q, Qian XD, Su YJ, Cai MJ (2000) 3-D chromatography of velocity structure in Tengchong volcano areas and nearby. J Seismol Res 23:157–164 (in Chinese with English abstract)
Roeder PL, Emslie RF (1970) Olivine-liquid equilibrium. Contrib Mineral Petrol 29:275–289
Seno T, Rehman HU (2011) When and why the continental crust is subducted: examples of Hindu Kush and Burma. Gondwana Res 19:327–333
Shervais JW (1982) Ti-V plots and the petrogenesis of modern ophiolitic lavas. Earth Planet Sci Lett 59:101–118
Socquet A, Pubellier M (2005) Cenozoic deformation in western Yunnan (China-Myanmar border). J Asian Earth Sci 24:495–515
Stephenson D (1984) The petrology and mineralogy of Mt. Popa volcano and the nature of the late-Cenozoic Burma volcanic arc. J Geol Soc Lond 141:747–762
Stolper E, Newman S (1994) The role of water in the petrogenesis of Mariana trough magmas. Earth Planet Sci Lett 121:293–325
Storey M, Saunders AD, Tarney J, Gibson IL, Norry MJ, Thirlwall MF, Leat P, Thompson RN, Menzies MA (1989) Contamination of Indian Ocean asthenosphere by the Kerguelen-Heard mantle plume. Nature 338:574–576
Sun S–S, McDonough WF (1989) Chemical and isotopic systematic of oceanic basalts: implications for mantle composition and processes. In: Saunders AD, Norry MJ (eds) Magmatism in the Ocean Basins. Geol Soc Lond Spec Pub 42:313–345
Széchenyi B (1893) Die wissenschaftliche Ergebnisse der Reise des Grafen Béla Széchenyi in Ost-Asien: 1877–1880
Tapponnier P, Peltzer G, Armijo R, Le Dain AY, Cobbold P (1982) Propagating extrusion tectonic in Asia: new insights from simple experiments with plasticine. Geology 10:611–616
Tatsumi Y (1986) Formation of the volcanic front in subduction zones. Geophys Res Lett 13:717–720
Taylor SR, McLennan SM (1985) The continental crust: its composition and evolution. Blackwell, Oxford, p 312
Tong W, Zhang MT (1989) Geothermal at Tengchong (in Chinese with English abstract). Science Press, Beijing, pp 20–31
Turner S, Arnaud N, Liu J, Rogers N, Hawkesworth C, Harris N, Kelley S, van Calsteren P, Deng W (1996) Post-collision, shoshonitic volcanism on the Tibetan Plateau: implications for convective thinning of the lithosphere and the source of ocean island basalts. J Petrol 37:45–71
van Westrenen W, Allan NL, Blundy JD, Purton JA (2000) Atomistic simulation of trace element incorporation into garnets-comparison with experimental garnet-melt partitioning data. Geochim Cosmochim Acta 64:1629–1639
Vervoort JD, Patchett PJ, Blichert-Toft J, Albarède F (1999) Relationships between Lu–Hf and Sm–Nd isotopic systems in the global sedimentary system. Earth Planet Sci Lett 168:79–99
Wang J-H, Yin A, Harrison TM, Grove M, Zhang Y-Q, Xie G-H (2001) A tectonic model for Cenozoic igneous activities in the eastern Indo-Asian collision zone. Earth Planet Sci Lett 188:123–133
Wang F, Peng Z, Zhu R, He H, Yang L (2006) Petrogenesis and magma residence time of lavas from Tengchong volcanic field (China): evidence from U series disequilibria and 40Ar/39Ar dating. Geochem Geophys Geosyst 7:Q01002. doi:10.1029/2005GC001023
Wang Y, Zhang X, Jiang C, Wei H, Wan J (2007) Tectonic controls on the late Miocene–Holocene volcanic eruptions of the Tengchong volcanic field along the southeastern margin of the Tibetan plateau. J Asian Earth Sci 30:375–389
Watson S (1993) Rare earth element inversions and percolation models for Hawaii. J Petrol 34:763–783
Weis D, Kieffer B, Maerschalk C, Pretorius W, Barling J (2005) High-precision Pb-Sr-Nd-Hf isotopic characterization of USGS BHVO-1 and BHVO-2 reference materials. Geochem Geophys Geosyst 6:Q02002
Williams HM, Turner SP, Pearce JA, Kelley SP, Harris NBW (2004) Nature of the source regions for post-collisional, potassic magmatism in southern and northern Tibet from geochemical variations and inverse trace element modelling. J Petrol 45:555–607
Xu HZ (1939) Tours of Xu Xiake (organized by Zhu ST and Wu US). Reproduced by Ancient Book Press, Shanghai, 1980
Xu YG, Lan JB, Yang QJ, Huang XL, Qiu HN (2008) Eocene break-off of the Neo-Tethyan slab as inferred from intraplate-type mafic dykes in the Gaoligong orogenic belt, eastern Tibet. Chem Geol 255:439–453
Yan DP, Zhou M-F, Wang CY, Xia B (2006) Structural and geochronological constraints on the tectonic evolution of the Dulong-Song Chay tectonic dome in Yunnan province, SW China. J Asian Earth Sci 28:332–353
Yang HJ, Frey FA, Clague DA (2003) Constraints on the source components of lavas forming the Hawaiian North Arch and Honolulu volcanic. J Petrol 44:603–627
Yang JH, Sun JF, Chen F, Wilde SA, Wu FY (2007) Sources and petrogenesis of late Triassic dolerite dikes in the Liaodong Peninsula: Implications for post-collisional lithosphere thinning of the eastern North China Craton. J Petrol 48:1973–1997
YBGMR (Yunnan Bureau of Geology and Mineral Resources) (1979) Tengchong geologic map (1:200000) (in Chinese)
Yin A, Harrison T (2000) Geologic evolution of the Himalayan—Tibetan orogen. Ann Rev Earth Plan Sci 28:211–280
Yin GM, Li SH (2000) The thermoluminescence dating of the last eruption of Tengchong volcano (in Chinese with English abstract). Earthq Res 23:12–17
Zhang HD (1924) Volcanoes. Business Press, Shanghai, p 68
Zhao D, Liu L (2010) Deep structure and origin of active volcanoes in China. Geosci Front 1:31–44
Zhao ZD, Mo XX, Luo ZH, Zhou S, Dong GC, Wang LL, Zhang FQ (2003) Subduction of India beneath Tibet: magmatism evidence. Earth-Science Frontier 10:149–158 (in Chinese)
Zhao C, Ran H, Chen KH (2006) Present-day magma chambers in Tengchong volcano area inferred from relative geothermal gradient. Acta Petrologica Sinica 22:1517–1528 (in Chinese with English abstract)

Zhao ZD, Mo XX, Dilek Y, Niu YL, DePaolo DJ, Robinson P, Zhu DC, Sun C, Dong G, Zhou S, Luo Z, Hou ZQ (2009) Geochemical and Sr-Nd-Pb-O isotopic compositions of the post-collisional ultrapotassic magmatism in SW Tibet: petrogenesis and implications for India intra-continental subduction beneath southern Tibet. Lithos 113:190–212

Zhou M-F, Zhao J-H, Qi L, Su W, Hu RZ (2006) Zircon U-Pb geochronology and elemental and Sr–Nd isotopic geochemistry of Permian mafic rocks in the Funing area, SW China. Contrib Mineral Petrol 151:1–19

Zhu BQ, Mao CX, Lugmair GW, Macdougall JD (1983) Isotopic and geochemical evidence for the origin of Plio-Pleistocene volcanic rocks near the Indo-Eurasian collisional margin at Tengchong, China. Earth Planet Sci Lett 65:263–275

Zindler A, Hart SR (1986) Chemical dynamics. Ann Rev Earth Plan Scis 14:493–571

Zou HB, Fan QC, Schmitt AK, Sui JL (2010) U-Th dating of zircons from Holocene potassic andesites (Maanshan volcano, Tengchong, SE Tibetan Plateau) by depth profiling: Time scales and nature of magma storage. Lithos 118:202–210